Transportation Geotechnics 52 (2025) 101582

Contents lists available at ScienceDirect

Transportation Geotechnics

journal homepage: www.elsevier.com/locate/trgeo

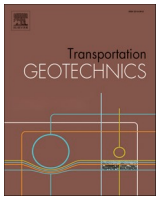

An insight into the stability of unsaturated embankments with different suction profiles

Leonardo Maria Lalicata [a,*], Gorizia D'Alessio [b], Francesca Casini [b]

[a] University of Genoa, Via Montallegro 1, 16145 Genova, Italy
[b] University of Rome, Tor Vergata, via del Politecnico 1, 00133 Roma, Italy

ARTICLE INFO

Keywords:
Unsaturated slopes stability
Limit equilibrium analysis
Infiltration
Stability charts
Water retention curve
Embankments

ABSTRACT

As-compacted soil embankments are partially saturated and, during their lifetime, they experience changes in water content and suction according to interaction with the atmosphere and the groundwater table. However, conventional slope stability assessments often assume either dry or fully saturated conditions, which can lead to inaccurate predictions. This paper presents an analytical framework for the analysis of the stability of unsaturated embankments under different suction profiles. The limit equilibrium analysis is extended to unsaturated slopes by incorporating matric suction, degree of saturation, and rainfall infiltration. A novel design chart is introduced to illustrate the interplay between the hydromechanical parameters of the slope, its geometry, the position of the groundwater table, and the infiltration profile. The outcomes demonstrate the significance of suction and saturation distributions in the sustainable planning and safety evaluation of embankments, offering meaningful perspectives for enhancing design methodologies and prevent failures in unsaturated engineered slopes. A key finding is the identification of the transition infiltration depth, which delineates the shift from deep to shallow slip surfaces. If the wetting front remains above this threshold, the design chart remains applicable. However, if it extends beyond this depth, a more comprehensive stability analysis is required. The method has been successfully used to predict the safety factor of engineered slopes under different suction profiles. Serving also as a benchmark for more advanced stability analyses, the design chart provides engineers with a practical tool for integrating unsaturated soil behaviour into geotechnical design, enhancing risk assessment and failure prevention strategies.

Introduction

Embankments are compacted at the optimum water content, resulting in a degree of saturation lower than one and a negative pore water pressure that sustains the pore structure through menisci. Nevertheless, the routine design and verification of these earth structures are typically performed using charts based on either fully saturated or dry conditions, in undrained or drained conditions [1–5]. Therefore, these charts need to be extended to properly account for partially saturated conditions and to incorporate the appropriate strength parameters for the design and verification of embankments. Partially saturated conditions increase soil strength and enhance the slope stability [6–12]. Rising groundwater table or water infiltration from the ground surface increase the degree of saturation and decrease the matric suction in the slope, which in turn may trigger an instability phenomenon [13–27].

For specific case studies, the stability of partially saturated slope and embankments can be analysed with the aid of commercial software (*e.g.* [28–31]). Conversely, a generic perspective of the role of soil partial saturation into the slope stability may be better investigated by design charts that correlate the factor of safety of the slope to its geometrical and hydro-mechanical parameters. Recently, some studies extended the design charts to unsaturated soil conditions only for the special case of slip surface emerging at the toe of the slope, and that does not intercept the groundwater table, specific soil types and water retention parameters. The proposed solutions in the literature differ for the assumed suction profile in the slope: Vahedifard et al. [32] and Sun et al. [33] considered a stationary suction distribution with possible crack formation, Vo and Russel [34] considered a linear contribution of suction for curvilinear slopes, and finally Huang et al. [35] and Huang [36] assumed a constant suction profile.

This paper fills the gap between the available solutions for

* Corresponding author.
E-mail address: leonardo.lalicata@unige.it (L.M. Lalicata).

https://doi.org/10.1016/j.trgeo.2025.101582
Received 31 July 2024; Received in revised form 29 April 2025; Accepted 5 May 2025
Available online 6 May 2025

unsaturated soil conditions to a more generalised solution, where the slip surface can either intercept the ground water table or emerge at the toe of the slope without any shape restrictions. For the first time, the stability charts are extended to unsaturated conditions considering the full range of slip surfaces and a wide range of soil types. To this end, and in absence of infiltration, a systematic investigation is performed on the coupling between the water retention curve, the suction profiles and the sliding resistance employing the extended Mohr-Coulomb failure criterion formulated in the Bishop's effective stress. This allows to directly consider the dependency of the soil strength on the water retention parameters, which is a fundamental feature to evaluate the safety factor in partially saturated embankments. Furthermore, the effect of water infiltration was studied by imposing different paradigmatic suction profiles above the water table. The method was satisfactorily validated against fully coupled hydromechanical finite element analysis, centrifuge tests [37], and field observations [16] under different initial conditions and rainfall events. The proposed solution was implemented in an open-access code, and stability charts are proposed as a function of nondimensional groups describing the water table position, the slope geometry, and the hydromechanical parameters of the soil.

Methodology

The stability of artificial slopes under unsaturated soil conditions was analysed using the method of the slices, following Bishop's approach [38] and assuming a circular slip surface. Over the years, the Bishop method has gained popularity due to its simplicity, the clear physical meaning of the parameters, and the good agreement with the experimental data [39]. Moreover, it is one of the limit equilibrium methods endorsed by Eurocode 7 (EN 1997-1) for the analysis of slope stability as discussed by Bond et al. [40]. As will be shown later, for circular slip surfaces, the safety factor values predicted by the Bishop method are virtually identical to those obtained using more rigorous slice methods, such as Morgenstern and Price method [41]. Therefore, the use of the Bishop method is fully justified for the purposes of this study. Taking advantage of the flexibility of the slices method, the solution has been implemented in a Python code, adopting the scheme in Fig. 1, where H is the height of the slope, β is the slope angle, H_w is the depth of the ground water table (GWT), measured from the toe of the slope and assumed horizontal for simplicity, and finally z_w is the infiltration depth that is parallel to the soil surface as suggested by Huang et al. [35] and Zhang et al. [42]. Notably, treating z_w as an input variable allows for the execution of the stability analysis alone, thereby eliminating the need for a transient seepage analysis to determine the pore pressure distribution within the slope. This procedure enables a greater generalisation of the results and the development of simple design charts, which can be used for a preliminary assessment of embankment stability under infiltration. Note also that, unlike other solutions available in the literature, the proposed method imposes no restrictions on the position of the slip surface, which can intersect both the groundwater table and the wetting front. The search algorithm used to determine the critical factor of safety of the slope combines a traditional grid-based search with the simplex method, ensuring an efficient minimisation process. The robustness of the minimisation algorithm adopted is discussed in detail in Lalicata et al. [43] for dry soil conditions.

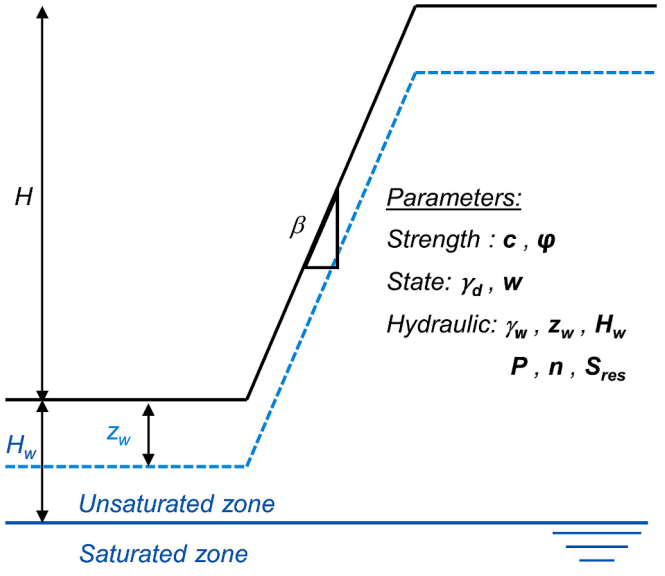

Fig. 1. Sketch of the geometry adopted in the calculation.

Paradigmatic infiltration profiles

Unsaturated soils are triphase materials consisting of solid grains separated by pores which are partially filled by gas (air) and partially filled by liquid (water), where the difference between pore air and water pressure is named matric suction, $s = u_a - u_w$ or simply suction (as in the following part of this paper). In field applications, the soil above the GWT is generally unsaturated and the air pressure is atmospheric (i.e. $u_a = 0$) while the pore water pressure is negative, meaning that suction is equal to pore water pressure changed of the sign. The actual distribution of pore water pressure above the GWT depends on the boundary conditions on the ground surface and, more specifically, on whether water infiltration or evaporation prevails.

The stability of an unsaturated soil slope is directly affected by the profiles of pore water pressure and the degree of saturation on the slope. In this study, two reference conditions have been identified; see Fig. 2: The first corresponds to a constant pore pressure profile representative of the as compacted conditions (i.e. short-term conditions for engineered slopes), and the second is a hydrostatic distribution of pore water pressure that is representative of idealised long-term conditions. Such profiles change upon infiltration where the suction reduces close to the ground surface. In this case, the pore water pressure and degree of saturation profiles are most appropriately obtained by finite element transient seepage analysis [44][16,22,28,45,46]. However, the application of such analysis in practice is limited because of the difficulty in obtaining some input parameters (such as the permeability law and rainfall data) and uncertainty in the initial and boundary conditions. An alternative is to use an infiltration model based on the wetting front concept that is proven to agree reasonably well with finite element transient seepage analysis [47–49] and measurement [50]. A detailed review of conceptual infiltration models can be found in Zhang et al. [42].

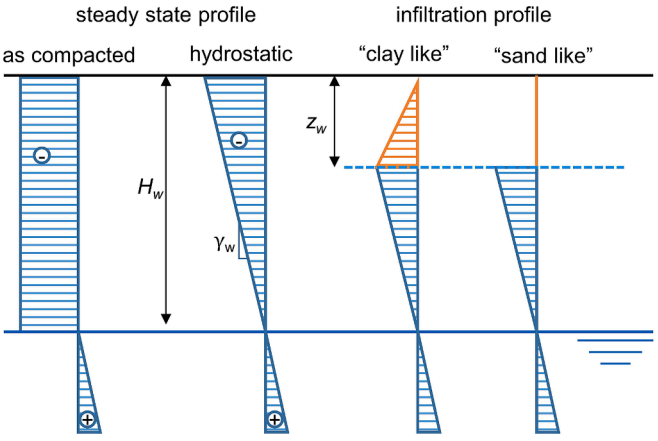

Fig. 2. Pore pressure distributions for the hydrostatic case, the "clay-like" and "sand-like" infiltration profiles.

The idealised pore water pressure profiles for the soil above the wetting front adopted in this study are shown in Fig. 2 and are like those suggested by Rahardjo et al. [51] and Huang et al. [35]. The *"clay-like"* profile represents a situation where suction is reduced to zero at the ground surface and then increases with depth until it intersect the initial hydrostatic value at the wetting front, z_w. Instead, in the *"sand like"* profile the suction above the wetting front is reduced to zero. These names derive from previous research showing that the first profile tends to occur in fine-grained soils, while the latter is typical of coarse-grained soils [48,49].

The depth of the wetting front z_w varies with time, intensity of the rainfall event, soil permeability, and initial degree of saturation in the soil; and can be calculated with any one-dimensional infiltration model [52–54]. However, in this study z_w is taken as an input variable and its determination is left to the reader. The reliability of the selected values of infiltration depth should be evaluated case by case according to the boundary conditions and hydraulic properties of the soil.

Physical and mechanical parameters in unsaturated soils

The increase in soil strength due to suction above the GWT is usually modelled by introducing an apparent cohesion [8,9,55–61]. The apparent cohesion can be obtained from the extended Mohr-Coulomb failure criterion (e.g. [62–64]) which calculates the soil shear strength τ_f in terms of the average skeleton stress σ' to account for partial saturation. The average skeleton stress σ' [65] is a particular form of Bishop stress [6] and is defined as:

$$\sigma' = (\sigma - u_a) + \chi\,(u_a - u_w) \tag{1}$$

where the Bishop parameter $\chi = \chi(S_r)$ is equal to 1 in fully saturated conditions and Eqn 1recovers the Terzaghi effective stress when the soil becomes saturated (i.e. $S_r = 1$). In this study, the Bishop parameter is taken equal to the effective degree of saturation S_e, although alternative solutions are possible [66–68]. S_e can then be recast as a function of suction through the Soil Water Retention Curve (SWRC). Among the many SWRCs proposed in the literature, the Van Genuchten [69] model is chosen and introduced in equation (2):

$$S_e = \left(1 + \left(\frac{s}{P}\right)^n\right)^{-m} \tag{2}$$

where P (kPa) approximates the air entry suction, the non-dimensional parameters n and m control instead the shape of the retention curve and m is related to n by the relationship $m = 1 - \frac{1}{n}$. In this study, the attention is focused on the wetting path upon rainfall, and the hydraulic hysteresis of the SWRC is neglected.

Finally, the degree of saturation S_r can be written as:

$$S_r = S_{res} + (1 - S_{res})S_e \tag{3}$$

where S_{res} is residual degree of saturation.

Thus, adopting $\chi = S_e$, the extended Mohr-Coulomb failure criterion is then:

$$\tau_f = c' + \sigma_n' \tan\varphi' = c' + (\sigma_n + S_e s)\tan\varphi' = c' + \sigma_n \tan\varphi' + S_e s \tan\varphi' \tag{4}$$

where τ_f is the shear strength, c' is the effective cohesion, $\sigma_n \tan\varphi'$ is the frictional soil strength depending on the total normal stress σ_n and the tangent of the friction angle $\tan\varphi'$, $S_e s \tan\varphi'$ is the frictional term due to partially saturated condition (often, and hereafter, named apparent cohesion). In the latter, s is the suction, S_e is the effective degree of saturation obtained with Eq. (2). The total normal stress σ_n depends on the unit weight of soil γ, which in turn is a function of the dry density γ_d and of the gravimetric water content w as:

$$\gamma = \gamma_d(1 + w) \tag{5}$$

Recently, Zhai et al. [29] demonstrated that incorporating the unsaturated unit weight in Eq. (5) can enhance slope stability by up to 10 % compared to standard analyses, which assume a constant unit weight within the slope. Zhai et al. [29] also indicated that the influence of unsaturated shear strength and unsaturated unit weight on the computed F values is more significant than the effect of 3D analyses compared to 2D analyses.

Fine graded soils retain large amounts of water at high suctions resulting in large values of P, and exhibit a gradual transition from saturated to dry conditions, resulting in small values of n. Coarse soils, on the contrary, exhibit small values of P and a steeper transition from saturated to dry conditions, which corresponds to large values of n. The dependency of the water retention curve on the void ratio is accounted with the parameter P. As the voids decreases, the soil is able to retain more water, resulting in an increase in the P value. Typical values of P and n for different soil categories and void ratio have been published by several authors [70][58,71–81] and are listed in Table 1, although larger values of n are sometimes quoted.

This methodology incorporates key principles of unsaturated soil mechanics into slope stability analysis (Eqs. (1)–(3), specifically by accounting for the increase in shear strength and the change in unit weight, as described in Equations (4) and (5). The influence of soil type and void ratio on the soil water retention curve is addressed through the selection of appropriate Van Genuchten parameters, as presented in Table 1.

Validation of infiltration profiles

The proposed infiltration profiles for clayey and sandy soils were validated by a fully coupled hydro-mechanical analysis, using the finite element program PLAXIS 2D. The slope, consisting of a homogeneous material, was 5 m high with an inclination of 30°, while the overall dimensions of the model, 22.60 m long and 10 m high, were chosen to avoid any influence of the boundary conditions on the failure mechanism. The GWT position was established at a depth of 3 m below the toe of the slope, imposing a constant hydraulic head condition at the base of the domain. The initial pore water pressure profile was assumed to be hydrostatic, while the lateral boundaries were modelled as permeable.

Infiltration profiles were obtained through fully coupled numerical analyses, applying uniform rainfall conditions at the ground surface. The rainfall intensity was set at 0.86 mm/day for the clay soil, corresponding to a q/K_{sat} ratio equal to 10, and 100 mm/day for the sand soil, representing an intense yet realistic event. The failure criterion adopted is the Mohr-Coulomb criterion extended to partially saturated soils using Bishop's effective stresses, see Eq. (4). The SWRC and hydraulic conductivity function (HCF) were both modelled using the Van Genuchten [69] method. The expression for SWRC is provided in Eq. (2), while the hydraulic conductivity function is given in Eqs. (6) and (7) below.

$$K_{unsat} = K_{sat} k_{rel} \tag{6}$$

$$k_{rel} = S_e^l \left((1 - \left(1 - S_e^{\frac{1}{m}}\right)^m\right)^2 \tag{7}$$

where K_{unsat} is the unsaturated hydraulic conductivity, K_{sat} is the saturated hydraulic conductivity, k_{rel} is the relative permeability, $m = 1 - 1/n$ and l, n are the model parameters.

Table 1
Typical parameter values of the Van Genuchten [69] SWRC values for different soil types.

Type of soil	Air entry value P (kPa)	Slope of the transition zone n (–)	Residual degree of saturation S_{res} (–)
Clayey	25–1000	1.05–1.7	0.1–0.2
Silty	10–100	1.3–2.7	0.08–0.15
Sandy	0.5–20	1.5–4.0	0.05–0.1

All the physical, mechanical, and hydraulic properties of the analysed soils are listed in Table 2.

The safety factor was computed using $c' - \varphi'$ reduction method implemented in the finite element code. In this method, the shear strength parameters (friction angle φ' and cohesion c') are progressively reduced until slope failure occurs. The safety factor is defined as the ratio of the available strength to the strength at failure and provides a measure of the overall stability of the slope [82,83].

Fig. 3a and c show the contours of pore water pressure at four different time steps for the sand and clay soil, respectively. The wetting front advances almost parallel to the ground surface profile, thus validating the assumed infiltration profile reported in Fig. 2. Fig. 3b and Fig. 3d show the contours of plastic deformation, highlighting the slip surfaces activated before and during the rainfall event. The continuous black line identifies the slip surfaces predicted by the limit-equilibrium (LE) analyses, showing a very good agreement with the results obtained by the finite element (FE) analyses. Notably, in comparison with existing solution in the literature, the proposed LE method is capable of detecting also a deep failure mechanism, as typically observed in clay soils and illustrated in Fig. 3d. A slight divergence in the shape of the slip surfaces can be attributed to the different methodologies used in the calculation. Unlike the limit equilibrium method (black continuous line), the $c' - \varphi$ reduction method, which is used in finite element (FE) analyses, allows different shapes with respect to the circumferential arcs.

Fig. 4 shows the pore water pressure profiles in the middle of the slope at the same time steps as in Fig. 3. During the rainfall event in a sand soil, the position of the wetting front is clearly identified by the constant pore water pressure value approaching zero up to the ground surface (Fig. 4a). On the contrary, in clay soil the pore pressure profile reduces linearly from 0 (at the ground surface) to the infiltration depth where it intersects the hydrostatic profile. Below the infiltration depth, the pore water pressures remain under hydrostatic conditions.

The evolution of the factor of safety (F) with the advancing wetting front, z_w, is presented in Fig. 5a and Fig. 5b for sand and clay soils, respectively. The limit equilibrium (LE) method, based on the simplified infiltration profiles, exhibits good agreement with the finite element (FE) results. For the sand case, the LE method indicates that F decreases gradually with z_w until reaching $F = 1.9$ at $z_w = 0.7$ m, followed by a steep reduction to a nearly constant value of$F \cong 1.9$ for $z_w > 1.2$ m. In contrast, for clay soil (Fig. 5b), F decreases gradually until $z_w \cong 2.5$ m after which the rate of reduction of F with z_w increases. These different trends are influenced by the pore pressure distribution above the infiltration depth z_w (see Fig. 4) and by its interaction with the slip surface. Specifically, when the wetting front reaches the depth of the slip surface, a steeper reduction in F occurs.

Table 3 lists the F values computed by FE and LE models at different infiltration depths. The average error is 4.7 % for sand and 1.4 % for clay soil, confirming the validity of the proposed methodology. In the FE analyses, F is evaluated via the strength reduction method; therefore, minor differences with the LE results are expected. Finally, the F values calculated with Bishop and Morgenstern and Price methods are virtually identical, with discrepancies of less than ± 0.2 %. Therefore, the Bishop method is adopted in the following analysis.

Table 2
Physical, mechanical and hydraulic properties of the soils used in the FEM analyses.

	SAND	CLAY
Soil Parameters		
Saturated unit weight γ_{sat} *(kN/m³)*	18	18
Unsaturated unit weight γ_{unsat} *(kN/m³)*	16	16
Effective friction angle φ *(°)*	33	28
Effective cohesion c' *(kPa)*	0	5
Young Modulus E' (MPa)	50	20
Saturated Hydraulic Conductivity K_{sat} *(m/s)*	$1e^{-5}$	$1e^{-8}$
SWRC – HCF		
Air Entry Value P *(kPa)*	5	200
Van Genuchten Parameter n *(–)*	1.80	1.56
Van Genuchten Parameter l (–)	0.50	0.50
Residual Saturation Degree S_{res} *(–)*	0.10	0.20

Validation against experimental data

Centrifuge tests from Ling et al. [37]

Ling et al. [37] investigated the stability of partially saturated compacted embankments using centrifuge testing. Two mixtures of Nevada sand and Speswhite kaolin clay were used to prepare the soil models, the first soil was prepared with 15 % fines by weight and the second with 30 % fines. The soil properties declared by the authors are listed in Table 4. The apparent cohesion c_{app} was used to back-calculate the suction, which was equal to 16.6 kPa and 40.2 kPa for the soils prepared with 15 % and 30 % fines respectively. As the water retention curve was not provided by the authors, χ was taken as equal to the degree of saturation (i.e. S_{res} was taken equal to 0) to avoid an additional source of uncertainty in the analysis.

In the centrifuge tests, gravity was progressively increased to induce the failure of the as-compacted soil slopes with different heights (10, 15, and 20 cm at the model scale) and slope inclinations (β = 60, 75 and 90°). In these tests, the water content profile with depth was constant, so that the soil could be assumed to be homogeneous with respect to suction and degree of saturation, see Table 4.

Fig. 6 shows the predicted safety factor F against the experimentally measured prototype height at failure, where F is equal to 1, for each value of β and fines content. Fig. 6 clearly demonstrates that most of the points fall within a ± 20 % error interval in terms of F-value confirming the good predictive capability of the limit equilibrium method proposed. The mean error and the standard deviation are 5 % (8 %) and 13 % (11 %) for the mixtures prepared with 15 % and 30 % fines, respectively. The difference between the measured ($F = 1$) and predicted values of the safety factor, shown in Fig. 6, could also be attributed to some degree of heterogeneity of soil properties related to the dynamic compaction procedure and/or moisture migration during flight, which were not considered in the analysis.

Case study of rainfall-induced cut-slope failure: Pohang Site [16]

Oh and Lu [16] back analysed the rainfall-induced failure of an engineered cut slope at the Pohang site in South Korea. The slope failed after a three-month rainfall of 420 mm, which, according to the authors, was typical at the Pohang site. The slope was 10 m high and the inclination of the two steps was ~ 40° with respect to the horizontal plane, the groundwater table was 2 m below the toe of the slope. In the calculation, the slope profile has been linearised as in Fig. 7, and the resulting inclination was$\beta = 38°$. The Pohang silty soils are weathered from mudstone and shale and contain more than 50 % fine-grained materials. Soil parameters derived from the site investigation and laboratory tests are reported in Table 5.

Oh and Lu [16] carried out a transient infiltration analysis to define the pore pressure distribution on the slope at the beginning of the three-month rainfall that induced failure. They found that the pore pressures were in hydrostatic equilibrium with the GWT, and such a profile was used in the stability analysis. Rainfall effects are simulated assuming the *"sand-like"* infiltration profile in Fig. 2 and the results are presented in Fig. 8. Due to the initial large value of F, the infiltration has little effect on the stability for$z_w < 1.5$ m but when a significant portion of the slope is fully saturated, F abruptly reduces from 1.95 to 0.85 when z_w deepens from 1.5 to 1.65 m. As shown in Fig. 8, for$z_w < 1.5$ m only a small portion of the critical slip surface is affected by the wetting front whilst most of the slip surface is still in the unsaturated and undisturbed zone. Conversely, for$z_w > 1.65$ m the whole length of the slip circle passes inside the wetted zone of the slope, so that all the additional strength provided by the partially saturated soil is lost and the slope becomes

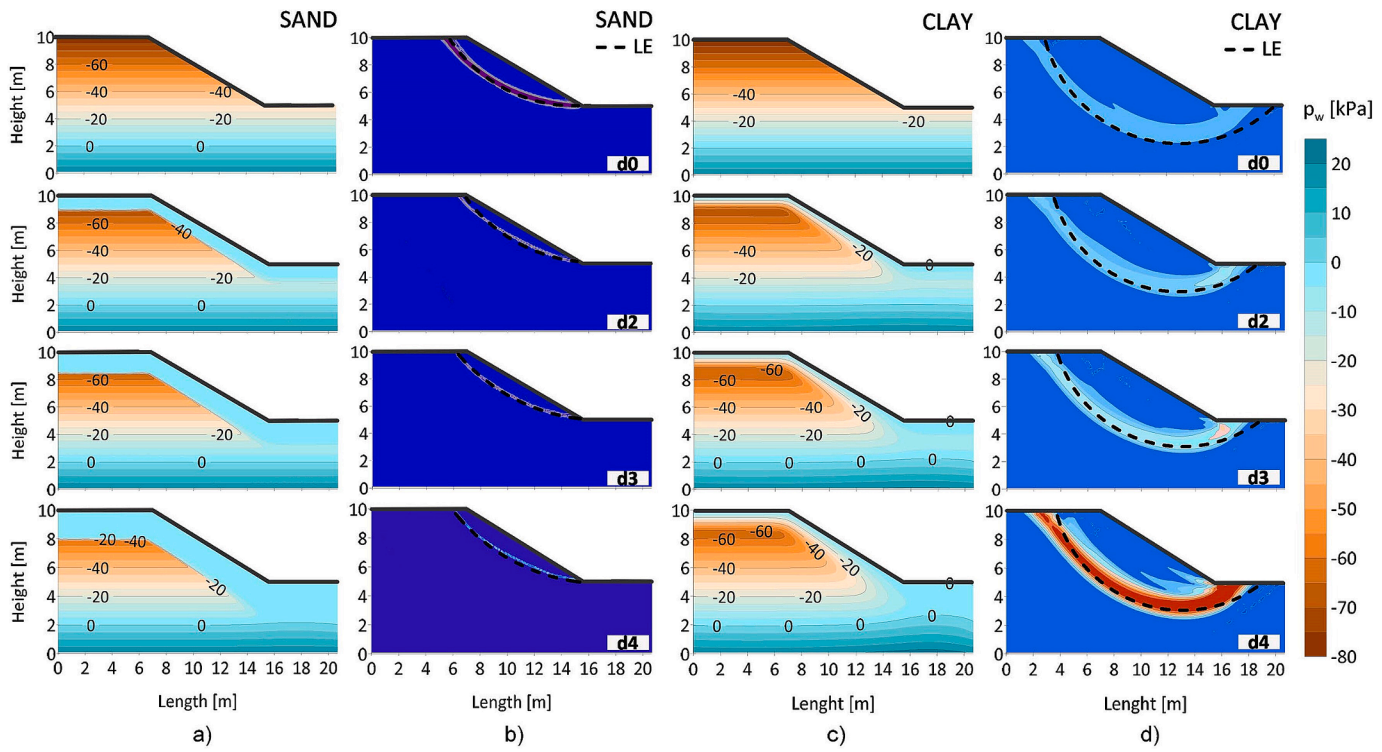

Fig. 3. Contours of the evolution of pore water pressure and plastic deformation during rainfall events: a, b) sand soil and c, d) clay soil.

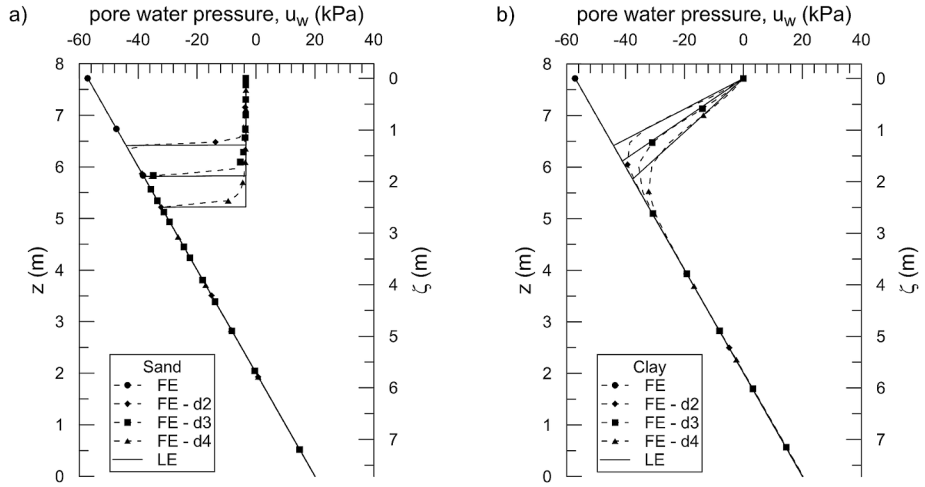

Fig. 4. Comparison between the pore pressure profile from 2D Finite Element analysis and the infiltration profile adopted in the Limit Equilibrium method for a) the sand slope and b) the clay slope.

unstable. The results are in substantial agreement with the transient stability analysis from Oh and Lu [16] which showed that in the upper part of the slope the pore pressures were ~ -5kPa while towards the bottom they ranged between 0 and 10 kPa, indicating a water table rising due to rainfall. Those features cannot be captured by the simplified infiltration analysis proposed in this work; however, the latter correctly predicts the slope instability when suction reduces to zero, as indicated by the more accurate transient analysis. The analysis is repeated also for the cut slope profile to explore the influence of the simplified geometry adopted in the analysis. The two trends are practically identical, with instability being triggered for the same value of z_w. Minor, and almost negligible differences are observed in the stable zone of Fig. 8, i.e. for low values of z_w, since the cut slope profile shows a slightly larger value of the safety factor in the stable zone. Conversely, values of the safety factor lower than 1 are predicted when $z_w > 1.65$ m for both the cut slope and the linearised profile.

Stability charts for partially saturated engineered slopes

as-compacted embankments

As-compacted embankments are characterised by a constant value of optimum dry density and water content, and therefore, by a constant apparent cohesion, see Eq. (4). Under these conditions, stability charts can be presented in a non-dimensional form in terms of $F/\tan\varphi'$ versus $c/\gamma H\tan\varphi'$ for any slope inclination β [3,36].

Fig. 9 shows the stability charts for β values ranging from 15° to 90° together with the range of the nondimensional material parameter,

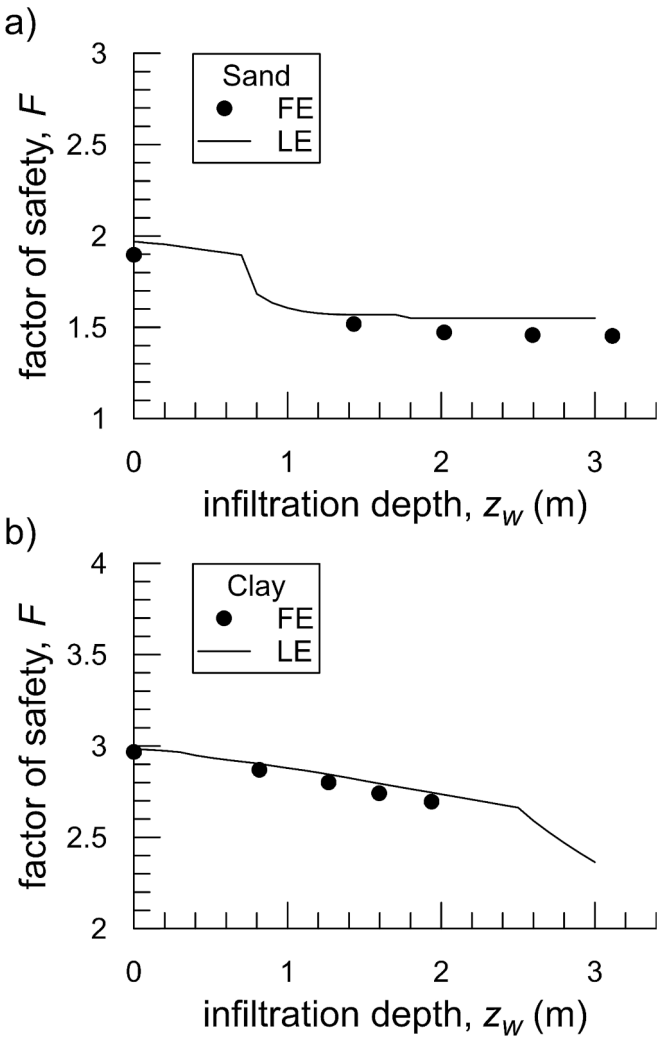

Fig. 5. Safety factor against infiltration depth: comparison between 2D Finite Element analysis and the Limit Equilibrium method for a) the sand slope and b) the clay slope.

Table 3
Comparison of the safety factor values obtained by the Finite Element (FE) model (c-φ' reduction) and the proposed Limit Equilibrium (LE) model at different infiltration depths z_w.

Soil type	z_w	Factor of Safety, F		
	(m)	FE	LE: Bishop	LE: Morgenstern and Price
sand	0	1.897	1.970	1.966
	1.4	1.518	1.569	1.567
	2.0	1.472	1.550	1.548
	2.6	1.457	1.550	1.548
clay	0	2.968	2.983	2.987
	1.3	2.801	2.840	2.840
	1.6	2.741	2.794	2.794
	1.9	2.695	2.743	2.742

$c/\gamma H\tan\varphi'$, evaluated for three different types of soils typically used as construction material and that are namely a sand, a silt and a clay according to the AASTHO norm [84]. The parameter $c/\gamma H\tan\varphi$ is limited to 5 because higher values are rarely encountered in practice. Note that $c = c' + S_e s\tan\varphi'$ (see Eq. (4)), and, for simplicity, c' is assumed equal to 0.

Typical values of optimum water content and dry density were selected based on embankment construction practices, while the range of as-compacted suction for each material was evaluated using the

Table 4
Soil properties from the Ling et al. [37].

Parameter	15 % fine	30 % fine
$G_s(-)$	2.666	2.661
$w(-)$	0.0766	0.087
$e(-)$	0.45	0.367
k_{sat}(cm/s)	1.8 10^{-5}	1.8 10^{-7}
φ (°)	43	41
c_{app}(kPa)	7	22
γ_d (kN/m^3)	18.02	18.98
$S_r(-)$	0.453	0.63
s(kPa)	16.6	40.2

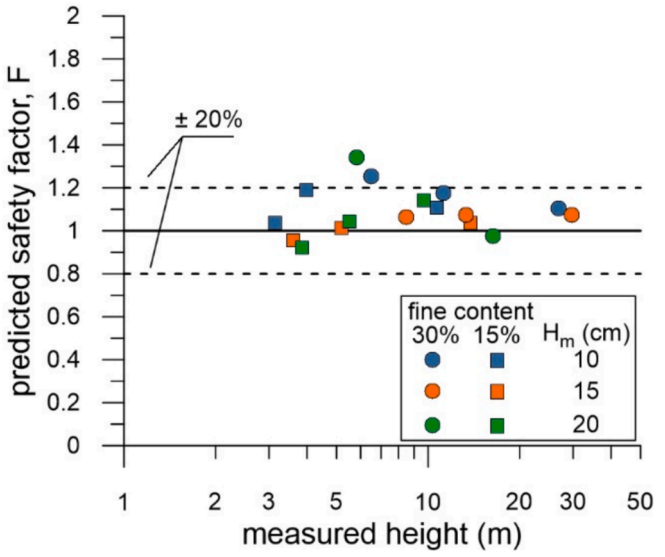

Fig. 6. Predicted safety factor for the measured slope heights at failure, at the prototype scale (data from [37].

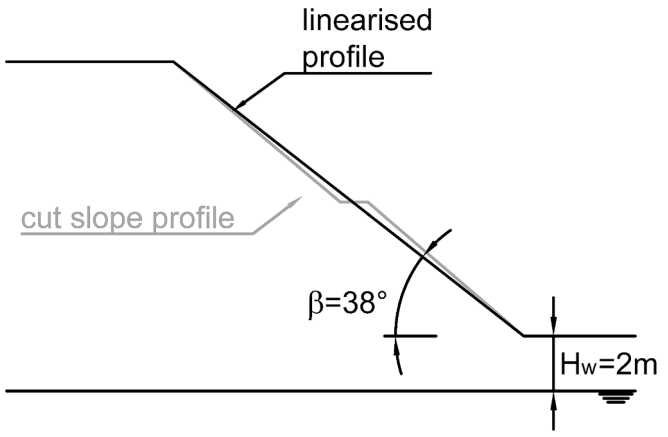

Fig. 7. Geometry adopted in the calculation, modified from Oh and Lu [16].

SWRC parameters ranges listed in Table 1. Finally, the non-dimensional material parameter was evaluated considering typical engineered slope heights values, from 2 to 10 m. All these values are summarised in Table 6. Notably, the nondimensional apparent cohesion is independent of the friction angle as the term $\tan\varphi'$ appears both in the numerator and in the denominator. Inspection of Table 6 reveals that, for clayey soils, the upper bound of the nondimensional apparent cohesion is exceptionally high, primarily due to the large values of air entry suction P (up to 1000 kPa) that clays can exhibit. However, these values correspond to very fine and highly active clays, which are unsuitable for construction

Table 5
Soil properties at the Pohang site Oh and Lu [16].

Specific gravity	Void ratio	Water content	Dry density	Effective cohesion	Friction angle	Saturated permeability	Residual degree of saturation	Air entry value	Slope of the VG model
G_s	e	w	γ_d (kN/m^3)	c' (kPa)	φ (°)	k_{sat}(m/s)	S_{res}	P(kPa)	n
2.65	0.866	0.296	13.93	0	32	3.46 x 10^{-6}	0.258	27.93	1.1

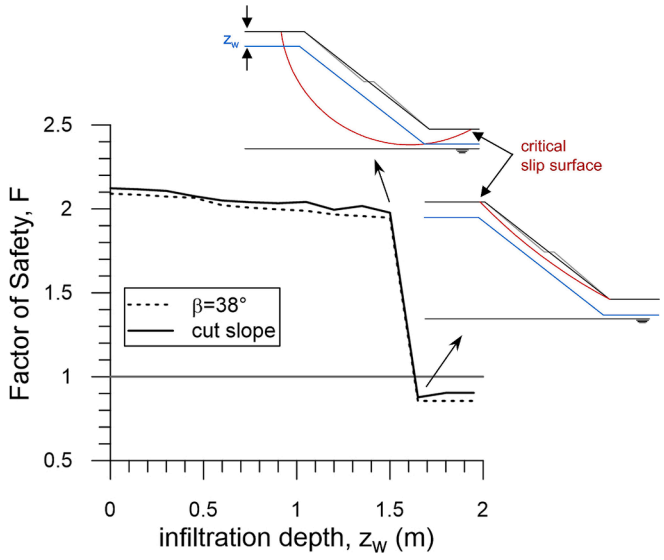

Fig. 8. Safety factor evolution with the advancing wetting front at the Pohang site.

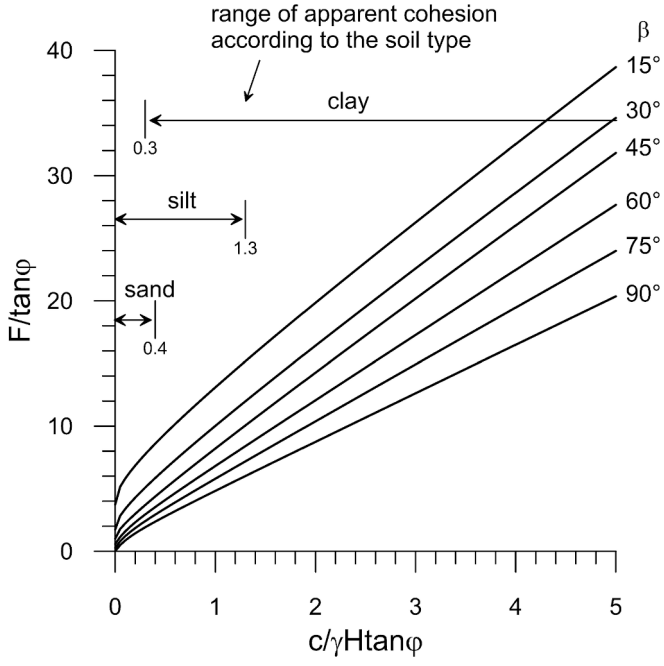

Fig. 9. Stability chart for partially saturated embankments.

purposes. Therefore, for practical applications and to maintain a conservative approach, a mean value of 4 can be considered.

The stability chart in Fig. 9 directly provides the normalised safety factor for a given embankment with inclination β, height H, and soil type. Due to its lower retention capacity, the strength increase in a partially saturated sand is significantly lower than that of a silt or clay,

Table 6
Typical values for as-compacted embankments.

Soil type	Optimum water content	Optimum dry density	Unit weight	Degree of saturation	Mean values of non-dimensional apparent cohesion *
	w(−)	γ_d (kN/m^3)	γ (kN/m^3)	S_r(−)	$S_e s/\gamma H$(−)
Sand	0.06	21.8	23.1	0.81	0.2 [0.01–0.4]
Silt	0.12	19.0	21.3	0.85	0.75 [0.03–1.3]
clay	0.16	17.5	20.3	0.86	4 [0.3–100]

*range in brackets.

as indicated by the upper bounds of non-dimensional apparent cohesion shown in Fig. 9. For example, in a silty soil, the influence of partial saturation, expressed by the non-dimensional apparent cohesion, $S_e s/\gamma H$, can range from 0 to 1.3 depending on the water retention parameters in Table 1. This means that, as an example, for a silty slope with $H = 5$ m and $\beta = 30°$, partial saturation can enhance stability by up to 590 % compared to dry conditions.

The stability chart can be used as long as the degree of saturation distribution can be assumed constant within the slope, i.e., under as-compacted conditions (short term), or when the water table is at a greater depth and the soil is close to hydraulic residual conditions. In all other cases, such as under hydrostatic conditions and upon infiltration or evaporation, the design chart in Fig. 9 is a priori no longer valid and a stability analysis with the appropriate pore pressure distribution is required.

An example of the effects of the infiltration profile is given in the following section.

Infiltration profiles

The influence of the different infiltration profiles on the stability of a slope with $H = 5$ m and $\beta = 60°$ is illustrated in Fig. 10 for the case of $H_w/H = 0.6$ and initial non dimensional apparent cohesion equal to 0.38. The two runs share the same hydromechanical parameters of the silty soil, see Table 6, so that the only difference is the infiltration profile. In the absence of infiltration, the safety factor F is equal to 1.78 ($F/tan\varphi' = 3.349$), which reduces upon infiltration. The reduction in F is shown in Fig. 10a and Fig. 10b as a function of apparent cohesion and infiltration depth, respectively.

Inspection of Fig. 10b shows that the *"sand-like"* profile leads to slope instability for $z_w/H > 0.18$ where $F/tan\varphi' = 0.577$. Notably, this value is equal to $1/tan\beta$ and corresponds to the safety factor of an infinite slope for a purely frictional soil. This is consistent with the infiltration profile that assumes zero suction above the infiltration depth. Conversely, the *"clay-like"* profile results in a slower reduction in the safety factor during infiltration because the suction within the wetting front, and hence the apparent cohesion, is not zero. At $z_w/H \sim 0.42$ there is a change in the rate of the safety factor evolution with z_w because, after that point, the whole sliding mass is comprised in the wetting front, where a significant reduction in available apparent cohesion occurs. This infiltration depth marking the transition between a slip surface not significantly affected by the wetting front and a slip surface entirely comprised within the wetting front is named transition infiltration

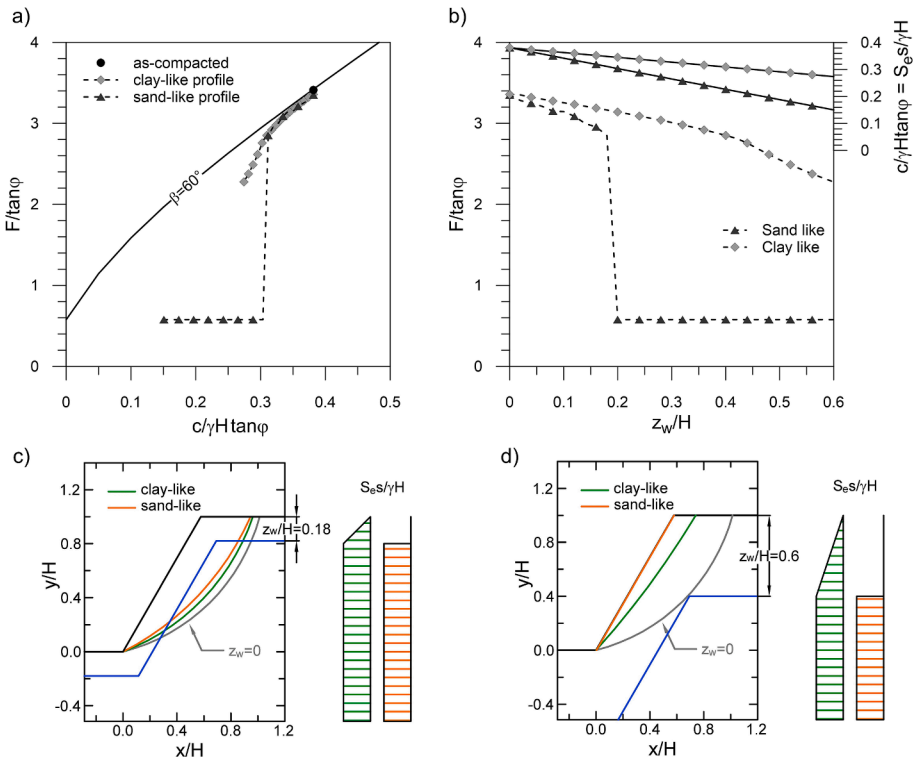

Fig. 10. Influence of the infiltration profile on a) stability chart, b) normalised factor of safety against the normalised infiltration depth, c) form of the slip surfaces for infiltration depth lower than the transition value, d) form of the slip surfaces for infiltration depth larger than the transition value.

depth, or simply transition depth hereafter. In the case analysed, the transition depth depends on the infiltration profile being equal to 0.2 H and 0.42 H for the "*sand-like*" and the "*clay-like*" infiltration profiles, respectively.

Fig. 10c and Figure 10d show the slip surfaces at different z_w/H values. Fig. 10c illustrates the case where the infiltration depth ($z_w/H = 0.18$) is lower than the transition value for both the "*sand-like*" and the "*clay-like*" infiltration profiles. In this case, a large portion of the slip surface extends beyond the wetting front for both infiltration profiles, meaning that the apparent cohesion along the slip surface is only marginally affected by the advancing wetting front. Therefore, the critical slip surface and the associated F-value remain similar to as-compacted conditions. Conversely, Fig. 10d represents the situation where the infiltration depth ($z_w/H = 0.6$) is larger than the transition value for both infiltration profiles. Here the wetting front is large enough to influence a significant portion of the slope height, the slip surface becomes shallower and is entirely contained within the wetting front.

Finally, Fig. 10a shows that when z_w/H is lower than the transition depth, the safety factor can still be evaluated with the stability chart by considering the apparent cohesion as the average value over the slope height, H. In this case, the difference between the stability chart and the stability analysis is less than 6 %. Conversely, when z_w/H exceeds the transition depth, the analysis deviates from the stability chart, requiring a more detailed stability analysis.

It is of practical interest to determine when the transition between deep and shallow failure surfaces occurs with respect to infiltration depth. This is analysed in Fig. 11 for the "*sand-like*" infiltration profile, which has been identified as the most critical for triggering slope instability, see Fig. 10, considering different apparent cohesion values. Fig. 11 shows that the transition infiltration depth increases with the slope angle β, ranging from $\sim$ 0.2 H for $\beta \leq 60°$ to 0.8 H for$\beta = 90°$, while being only marginally affected by the as-compacted apparent cohesion. The shallow failure surface corresponds to the infinite slope mechanism for a purely frictional soil and therefore, this is critical only if φ is lower than β, i.e. $F = tan\varphi/tan\beta < 1$. Note also that this result is

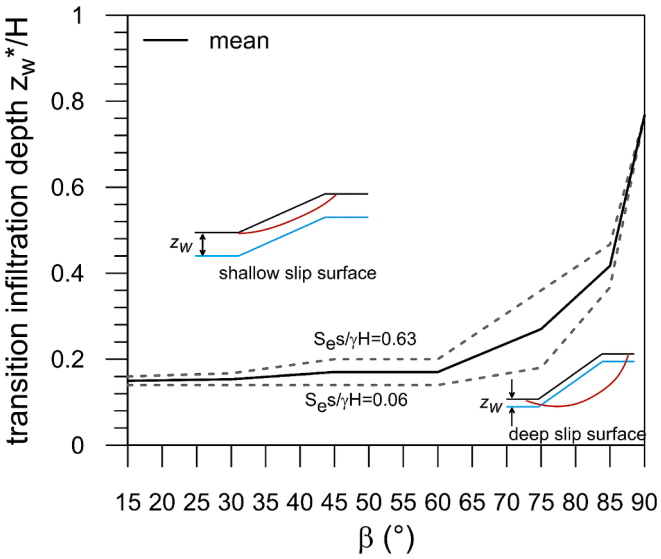

Fig. 11. Transition infiltration depth for a sand-like infiltration profile.

valid only if the pore pressures remain equal to 0 inside the wetting front, as assumed in this work.

Conclusions

The stability of partially saturated embankments was investigated using the slices method under different suction profiles using an in-house code and results were summarised in a non-dimensional design chart. In the partially saturated layer, the shear resistance is given by an extended Mohr-Coulomb criterion adopting the Bishop's effective stress. Rainfall effects were assessed by imposing different paradigmatic

suction profiles above the water table. The proposed design chart is derived from a general formulation of the slip surface, which can intersect both the groundwater table and the wetting front. Moreover, by using the infiltration depth as an input parameter, the methodology avoids the need for a transient seepage analysis, while still capturing the evolution of the factor of safety during infiltration events with good accuracy in comparison with fully coupled hydromechanical finite element analyses. This represents a notable advancement over existing solutions that typically assume stationary flow conditions and vertical infiltration only. This approach was successfully validated against also against centrifuge tests, and field observations under different initial conditions, rainfall events and geometries of the embankments.

During infiltration, there exists a transition infiltration depth at which the failure mechanism changes from a deeper failure to a shallower one, shifting closer to the ground surface. This transition depth is primarily influenced by the infiltration profile and the slope inclination. If the wetting front remains shallower than this transition depth, the design chart provided remains valid, with a negligible error compared the LEM results. Conversely, if the wetting front exceeds this threshold, a comprehensive stability analysis becomes necessary.

Despite its simplicity, the adoption of paradigmatic, and yet physically based, suction profile offers a rapid estimate of the critical conditions of a slope subjected to rainfall. The proposed method has the potential to serve as a benchmark for more advanced slope stability analyses, thereby offering an insight into the effects of unsaturated soil properties on slope stability. This can be particularly useful at both the design and verification stage.

CRediT authorship contribution statement

Leonardo Maria Lalicata: Writing – review & editing, Writing – original draft, Visualization, Validation, Software, Methodology, Investigation, Formal analysis, Data curation, Conceptualization. **Gorizia D'Alessio:** Writing – original draft, Validation, Software, Investigation. **Francesca Casini:** Writing – review & editing, Supervision, Project administration, Methodology, Formal analysis, Conceptualization.

Declaration of competing interest

The authors declare that they have no known competing financial interests or personal relationships that could have appeared to influence the work reported in this paper.

Acknowledgement

The second author acknowledges MUR for supporting her fellowship through the PNRR-M4C1/DM 351 (09/04/2022).

Data availability

Data will be made available on request.

References

[1] Taylor DW. Stability of earth slopes. J Boston Soc Civil Eng 1937;XXIV(3):337–86.
[2] Chen WF. *Limit Analysis and Soil Plasticity*. Amsterdam, Netherlands: Elsevier Science; 1975.
[3] Michalowski RL. Stability charts for uniform slopes. *J Geotech Geoenviron Eng* 2002; 128(4):351–5. https://doi.org/10.1061/(ASCE)1090-0241(2002)128:4(351).
[4] Baker R, Shukha R, Operstein V, Frydman S. Stability charts for pseudo-static slope stability analysis. Soil Dynamics and Earthquake Engineering 2006;26(9):813–23. https://doi.org/10.1016/j.soildyn.2006.01.023.
[5] Steward T, Sivakugan N, Shukla SK, Das BM. Taylor's Slope Stability Charts Revisited. International Journal of Geomechanics 2011;11(4):348–52. https://doi.org/10.1061/(ASCE)GM.1943-5622.0000093.
[6] Bishop AW, Blight GE. Some aspects of effective stress in saturated and partly saturated soils. *Géotechnique* 1963;13(3):177–97. https://doi.org/10.1680/geot.1963.13.3.177.
[7] Fredlund DG, Rahardjo H. Soil mechanics for unsaturated soils. New York: Wiley; 1993.
[8] Vanapalli SK, Fredlund DG, Pufahl DE, Clifton AW. Model for the prediction of shear strength with respect to soil suction. *Can Geotech J* 1996;33(3):379–92. https://doi.org/10.1139/t96-060.
[9] Lu N, Likos WJ. *Unsaturated soil mechanics*. New York: John Wiley & Sons; 2004.
[10] Laloui L, Nuth M. On the use of the generalised effective stress in the constitutive modelling of unsaturated soils. *Comput Geotech* 2009;36(1–2):20–3. https://doi.org/10.1016/j.compgeo.2008.03.002.
[11] Wang L, Gao Y, Zhou E, Feng J, Huang A, Xu M. Pseudo-static analysis of 3D unsaturated bench slopes stabilized by multiple rows of piles. *Transp Geotech* 2024; 46:1–11. https://doi.org/10.1016/j.trgeo.2024.101255.
[12] Xie Y, Feng SJ, Xiong YL, Zhang LL, Ye GL. Coupled hydraulic-mechanical-air simulation of unsaturated railway embankment under rainfall and dynamic train load. *Transp Geotech* 2021;27:1–11. https://doi.org/10.1016/j.trgeo.2020.100463.
[13] Rahardjo H, Lee TT, Leong EC, Rezaur RB. Response of a residual soil slope to rainfall. *Can Geotech J* 2005;42(2):340–51. https://doi.org/10.1139/t04-101.
[14] Cascini L, Cuomo S, Pastor M, Sorbino G. Modeling of rainfall-induced shallow landslides of the flow-type. *J Geotech Geoenviron Eng* 2010;136(1):85–98. https://doi.org/10.1061/(ASCE)GT.1943-5606.0000182.
[15] Eichenberger J, Ferrari A, Laloui L. Early warning thresholds for partially saturated slopes in volcanic ashes. *Comput Geotech* 2013;49:79–89. https://doi.org/10.1016/j.compgeo.2012.11.002.
[16] Oh S, Lu N. Slope stability analysis under unsaturated conditions: case studies of rainfall-induced failure of cut slopes. *Eng Geol* 2015;184:96–103. https://doi.org/10.1016/j.enggeo.2014.11.007.
[17] Bandara S, Ferrari A, Laloui L. Modelling landslides in unsaturated slopes subjected to rainfall infiltration using material point method: modelling landslides in unsaturated slopes subjected to rainfall infiltration using material point method. *Int J Numer Anal Meth Geomech* 2016;40(9):1358–80. https://doi.org/10.1002/nag.2499.
[18] Regmi RK, Jung K, Nakagawa H, Do XK, Mishra BK. Numerical analysis of multiple slope failure due to rainfall: Based on laboratory experiments. *Catena* 2017;150: 173–91. https://doi.org/10.1016/j.catena.2016.11.007.
[19] Rosone M, Ziccarelli M, Ferrari A, Farulla CA. On the reactivation of a large landslide induced by rainfall in highly fissured clays. *Eng Geol* 2018;235:20–38. https://doi.org/10.1016/j.enggeo.2018.01.016.
[20] Wang B, Vardon PJ, Hicks MA. Rainfall-induced slope collapse with coupled material point method. *Eng Geol* 2018;239:1–12. https://doi.org/10.1016/j.enggeo.2018.02.007.
[21] Lee W-L, Martinelli M, Shieh C-L. Modelling rainfall-induced landslides with the material point method: The Fei Tsui Road case. In: *Proceedings of the XVII European Conference on Soil Mechanics and Geotechnical Engineering, Geotechnical Engineering, foundation of the future*; 2019. p. 1835–42. https://doi.org/10.32075/17ECSMGE-2019-0346.
[22] Liu X, Wang Y, Li D-Q. Numerical simulation of the 1995 rainfall-induced Fei Tsui Road landslide in Hong Kong: New insights from hydro-mechanically coupled material point method. *Landslides* 2020;17(12):2755–75. https://doi.org/10.1007/s10346-020-01442-2.
[23] Sitarenios P, Casini F. The Hydromechanical Interplay in the Simplified Three-Dimensional Limit Equilibrium Analyses of Unsaturated Slope Stability. Geosciences 2021;11(2):73. https://doi.org/10.3390/geosciences1102007.
[24] Sitarenios P, Casini F, Askarinejad A, Springman S. Hydro-mechanical analysis of a surficial landslide triggered by artificial rainfall: the Ruedlingen field experiment. *Géotechnique* 2021;71(2):96–109. https://doi.org/10.1680/jgeot.18.P.188.
[25] Cascini L, Scoppettuolo MR, Babilio E. Forecasting the landslide evolution: From theory to practice. *Landslides* 2022;19(12):2839–51. https://doi.org/10.1007/s10346-022-01934-3.
[26] Pirone M, Di Maio R, Forte G, De Paola C, Di Marino E, Salone R, et al. Study of the groundwater regime in unsaturated slopes prone to landslides by multidisciplinary investigations: experimental study and numerical modelling. *Eng Geol* 2023;315: 107045. https://doi.org/10.1016/j.enggeo.2023.107045.
[27] Dodaro E, Giretti D, Pirone M, Ventini R, Zarattini F, Fioravante V, Gabrieli F, Gottardi G, Mancuso C, Simonini P. Centrifuge modelling of river embankments on homogeneous and layered subsoil| Modellazione fisica in centrifuga geotecnica di argini fluviali su sottosuolo omogeneo e stratificato. RIVISTA ITALIANA DI GEOTECNICA 2024;58(4):81–101. https://doi.org/10.19199/2024.4.0557-1405.102.
[28] Cuomo S, Di Perna A, Martinelli M. Modelling the spatio-temporal evolution of a rainfall-induced retrogressive landslide in an unsaturated slope. *Eng Geol* 2021; 294:106371. https://doi.org/10.1016/j.enggeo.2021.106371.
[29] Zhai Q, Tian G, Ye W, Rahardjo H, Dai G, Wang S. Evaluation of unsaturated soil slope stability by incorporating soil-water characteristic curve. *Geomech Eng* 2022; 28(6):637–44. https://doi.org/10.12989/gae.2022.28.6.637.
[30] Fraccica A, Romero E, Fallas JE. The impact of soil-vegetation-atmosphere interaction on a landslide initiation under torrential storms: a case study 2023;Vol. 382:06004.
[31] Schulz-Poblete M, van der Merwe F, Pequenino F. Unsaturated modelling, testing and monitoring towards the rehabilitation of a slope on National Route 3, KwaZulu-Natal, South Africa, Vol. 382. EDP Sciences; 2023.
[32] Vahedifard F, Leshchinsky D, Mortezaei K, Lu N. Effective stress-based limit-equilibrium analysis for homogeneous unsaturated slopes. *Int J Geomech* 2016;16 (6):D4016003. https://doi.org/10.1061/(ASCE)GM.1943-5622.0000554.
[33] Sun D, Wang L, Li L. Stability of unsaturated soil slopes with cracks under steady-infiltration conditions. *Int J Geomech* 2019;19(6):04019044. https://doi.org/10.1061/(ASCE)GM.1943-5622.0001398.

[34] Vo T, Russell AR. Stability charts for curvilinear slopes in unsaturated soils. *Soils Found* 2017;57(4):543–56. https://doi.org/10.1016/j.sandf.2017.06.005.
[35] Huang W, Leong E-C, Rahardjo H. Upper-bound limit analysis of unsaturated soil slopes under rainfall. *J Geotech Geoenviron Eng* 2018;144(9):04018066. https://doi.org/10.1061/(ASCE)GT.1943-5606.0001946.
[36] Huang W. Stability of homogeneous slopes: from chart to closed-form solutions and from deterministic to probabilistic analysis. *Int J Geomech* 2023;23(9):04023136.
[37] Ling HI, Wu M-H, Leshchinsky D, Leshchinsky B. Centrifuge modeling of slope instability. *J Geotech Geoenviron Eng* 2009;135(6):758–67. https://doi.org/10.1061/(ASCE)GT.1943-5606.0000024.
[38] Bishop AW. The use of the Slip Circle in the Stability Analysis of Slopes. *Géotechnique* 1955;5(1):7–17. https://doi.org/10.1680/geot.1955.5.1.7.
[39] Duncan JM. State of the art: limit equilibrium and finite-element analysis of slopes. *J Geotech Eng* 1996;122(7):577–96. https://doi.org/10.1061/(ASCE)0733-9410(1996)122:7(577).
[40] Bond AJ, Schuppener B, Scarpelli G, Orr TLL. Eurocode 7 geotechnical design: worked examples. Joint Research Centre, Institute for the Protection and Security of the Citizen. In: Dimova S, Pinto A, Nikolova B, editors. Publications Office, 2013, https://data.europa.eu/doi/10.2788/3398.
[41] Morgenstern NR, Price VE. The analysis of the stability of general slip surfaces. *Géotechnique* 1965;15(1):79–93. https://doi.org/10.1680/geot.1965.15.1.79.
[42] Zhang LL, Zhang J, Zhang LM, Tang WH. Stability analysis of rainfall-induced slope failure: a review. Proc Inst Civil Eng - Geotechn Eng 2011;164(5):299–316. https://doi.org/10.1680/geng.2011.164.5.299.
[43] Lalicata LM, Bressan A, Pittaluga S, Tamellini L, Gallipoli D. An efficient slope stability algorithm with physically consistent parametrisation of slip surfaces. *Int J Civ Eng* 2024. https://doi.org/10.1007/s40999-024-01053-1.
[44] Cai F, Ugai K. Numerical analysis of rainfall effects on slope stability. *Int J Geomech* 2004;4(2):69–78. https://doi.org/10.1061/(ASCE)1532-3641(2004)4:2(69).
[45] Rotisciani GM, Sciarra G, Casini F, Desideri A. Hydro-mechanical response of collapsible soils under different infiltration events. *Int J Numer Anal Meth Geomech* 2015;39(11):1212–34. https://doi.org/10.1002/nag.2359.
[46] Zhang LL, Fredlund DG, Fredlund MD, Wilson GW. Modeling the unsaturated soil zone in slope stability analysis. *Can Geotech J* 2014;51(12):1384–98. https://doi.org/10.1139/cgj-2013-0394.
[47] Sun HW, Wong HN, Ho KKS. Analysis of infiltration in unsaturated ground. In: Li KS, Kay JN, Ho KKS, editors. *Slope engineering in Hong Kong*. Rotterdam, The Netherlands: A.A. Balkema; 1998. p. 101–9.
[48] Lee LM, Gofar N, Rahardjo H. A simple model for preliminary evaluation of rainfall-induced slope instability. *Eng Geol* 2009;108(3–4):272–85. https://doi.org/10.1016/j.enggeo.2009.06.011.
[49] Zhang LL, Fredlund DG, Zhang LM, Tang WH. Numerical study of soil conditions under which matric suction can be maintained. *Can Geotech J* 2004;41(4):569–82. https://doi.org/10.1139/t04-006.
[50] Li AG, Yue ZQ, Tham LG, Lee CF, Law KT. Field-monitored variations of soil moisture and matric suction in a saprolite slope. *Can Geotech J* 2005;42(1):13–26. https://doi.org/10.1139/t04-069.
[51] Rahardjo H, Lim TT, Chang MF, Fredlund DG. Shear-strength characteristics of a residual soil. *Can Geotech J* 1995;32(1):60–77. https://doi.org/10.1139/t95-005.
[52] Lumb P. Slope failures in Hong Kong. *Q J Eng Geol Hydrogeol* 1975;8(1):31–65. https://doi.org/10.1144/GSL.QJEG.1975.008.01.02.
[53] Tracy FT. L-D, 2-D, and 3-D analytical solutions of unsaturated flow in groundwater. *J Hydrol* 1995.
[54] Godt JW, Şener-Kaya B, Lu N, Baum RL. Stability of infinite slopes under transient partially saturated seepage conditions: transient unsaturated landslides. *Water Resour Res* 2012;48(5). https://doi.org/10.1029/2011WR011408.
[55] Fredlund DG, Xing A, Fredlund MD, Barbour SL. The relationship of unsaturated soil shear strength to the soil– water characteristic curve. Can Geotech J 1996;33:440–8.
[56] Hamid TB, Miller GA. Shear strength of unsaturated soil interfaces. *Can Geotech J* 2009;46(5):595–606. https://doi.org/10.1139/T09-002.
[57] Melinda F, Rahardjo H, Han KK, Leong EC. Shear strength of compacted soil under infiltration condition. J Geotech Geoenviron Eng ASCE 2004;130(8):807–17.
[58] Vahedifard F, Leshchinsky BA, Mortezaei K, Lu N. Active Earth Pressures for Unsaturated Retaining Structures. *J Geotech Geoenviron Eng* 2015;141(11):04015048. https://doi.org/10.1061/(ASCE)GT.1943-5606.0001356.
[59] Zhou A, Huang R, Sheng D. Capillary water retention curve and shear strength of unsaturated soils. *Can Geotech J* 2016;53(6):974–87. https://doi.org/10.1139/cgj-2015-0322.
[60] Kim BS, Park SW, Lohani TN, Kato S. Characterizing suction stress and shear strength for unsaturated geomaterials under various confining pressure conditions. *Transp Geotech* 2022;34:1–11. https://doi.org/10.1016/j.trgeo.2022.100747.
[61] Lalicata LM, Bruno AW, Gallipoli D. An extension of Broms' theory to unsaturated soils. *Comput Geotech* 2023;155:105189. https://doi.org/10.1016/j.compgeo.2022.105189.
[62] Gallipoli D, Gens A, Chen G, D'Onza F. *Comput Geotech* 2008;35(6):825–34. https://doi.org/10.1016/j.compgeo.2008.08.006.
[63] Sheng D, Zhou A, Fredlund DG. Shear Strength Criteria for Unsaturated Soils. Geotech Geol Eng 2011;29:145–59.
[64] Tarantino A, Di Donna A. Mechanics of unsaturated soils: Simple approaches for routine engineering practice. Rivista Italiana di Geotecnica 2019;4:5–46. https://doi.org/10.19199/2019.4.0557-1405.005.
[65] Jommi C. Remarks on the constitutive modelling of unsaturated soils. *Experimental Evidence and Theoretical Approaches in Unsaturated Soils*. CRC Press; 2000.
[66] Khalili NGFA, Geiser F, Blight GE. Effective stress in unsaturated soils: Review with new evidence. *Int J Geomech* 2004;4(2):115–26.
[67] Alonso EE, Pereira J-M, Vaunat J, Olivella S. A microstructurally based effective stress for unsaturated soils. *Géotechnique* 2010;60(12):913–25. https://doi.org/10.1680/geot.8.P.002.
[68] Vaunat J, Casini F. A procedure for the direct determination of Bishop's χ parameter from changes in pore size distribution. *Géotechnique* 2017;67(7):631–6. https://doi.org/10.1680/jgeot.15.T.016.
[69] van Genuchten MT. A closed-form equation for predicting the hydraulic conductivity of unsaturated soils. *Soil Sci Soc Am J* 1980;44(5):892–8. https://doi.org/10.2136/sssaj1980.03615995004400050002x.
[70] Dodaro E, Sorrentino G, Ventini R, Viggiani GM, Gottardi G, Mancuso C. A suction-controlled laboratory campaign for assessing the hydro-mechanical properties of a compacted silty sand mixture. Rivista Italiana di Geotecnica 2024;58(4):102–24. https://doi.org/10.19199/2024.4.0557-1405.102.
[71] Gallipoli D, Wheeler SJ, Karstunen M. Modelling the variation of degree of saturation in a deformable unsaturated soil. *Géotechnique* 2003;53(1):105–12.
[72] Tarantino A, De Col E. Compaction behaviour of clay. *Géotechnique* 2008;58(3):199–213. https://doi.org/10.1680/geot.2008.58.3.199.
[73] Romero E, Della Vecchia G, Jommi C. An insight into the water retention properties of compacted clayey soils. *Géotechnique* 2011;61(4):313–28. https://doi.org/10.1680/geot.2011.61.4.313.
[74] Casini F. Deformation induced by wetting: a simple model. *Can Geotech J* 2012;49(8):954–60. https://doi.org/10.1139/t2012-054.
[75] Likos WJ, Lu N, Godt JW. Hysteresis and uncertainty in soil water-retention curve parameters. *J Geotech Geoenviron Eng* 2014;140(4):04013050. https://doi.org/10.1061/(ASCE)GT.1943-5606.0001071.
[76] Soranzo E, Tamagnini R, Wu W. Face stability of shallow tunnels in partially saturated soil: centrifuge testing and numerical analysis. *Géotechnique* 2015;65(6):454–67. https://doi.org/10.1680/geot.14.P.123.
[77] Lu N. Generalized Soil Water Retention Equation for Adsorption and Capillarity. *J Geotech Geoenviron Eng* 2016;142(10):04016051. https://doi.org/10.1061/(ASCE)GT.1943-5606.0001524.
[78] Rotisciani GM, Casini F, Desideri A, Sciarra G. Hydromechanical behavior of an embankment during inundation. *Can Geotech J* 2017;54(3):348–58. https://doi.org/10.1139/cgj-2016-0174.
[79] Lalicata LM, Rotisciani GM, Desideri A, Casini F, Thorel L. Physical modelling of piles under lateral loading in unsaturated soils. *E3S Web Conf* 2020;195(01021). https://doi.org/10.1051/e3sconf/202019501021.
[80] Lalicata LM, Rotisciani GM, Desideri A, Casini F. A numerical model to study the response of piles under lateral loading in unsaturated soils. *Geosciences* 2022;12(1). https://doi.org/10.3390/geosciences12010001.
[81] Rotisciani GM, Lalicata LM, Desideri A, Casini F. Numerical modelling of the response of an unsaturated silty soil under wetting and gravitational loading processes. *E3S Web Conf* 2020;195:02012. https://doi.org/10.1051/e3sconf/202019502012.
[82] Matsui T, San KC. Finite element slope stability analysis by shear strength reduction technique. *Soils Found* 1992;32(1):59–70.
[83] Dawson EM, Roth WH, Drescher A. Slope stability analysis by strength reduction. *Geotechnique* 1999;49(6):835–40. https://doi.org/10.1680/geot.1999.49.6.835.
[84] UNI EN 13286-2. Unbound and hydraulically bound mixtures - part 2: test methods for laboratory reference density and water content - proctor compaction. Ente Nazionale di Unificazione (UNI); 2010.